Neutron physics of the Re/Os clock. II. The (n,n') cross section of ^{187}Os at 30 keV neutron energy

M. Mosconi,* M. Heil,† F. Käppeler, and R. Plag†
Karlsruhe Institute of Technology (KIT), Campus Nord, Institut für Kernphysik, D-76021 Karlsruhe, Germany

A. Mengoni
International Atomic Energy Agency, Nuclear Data Section, A-1400 Vienna, Austria
(Received 14 December 2009; published 15 July 2010)

The inelastic neutron-scattering cross section of ^{187}Os has been determined in a time-of-flight experiment at the Karlsruhe 3.7-MV Van de Graaff accelerator. An almost monoenergetic beam of 30-keV neutrons was produced at the threshold of the ^{7}Li$(p,n)^{7}$Be reaction. Information on the inelastic channel is required for reliable calculations of the so-called stellar enhancement factor, by which the laboratory cross section of ^{187}Os must be corrected in order to account for the thermal population of low-lying excited states at the temperatures of s-process nucleosynthesis, in particular of the important state at 9.75 keV. This correction represents a crucial step in the interpretation of the ^{187}Os/^{187}Re pair as a cosmochronometer.

DOI: 10.1103/PhysRevC.82.015803 PACS number(s): 25.40.Fq, 26.20.Kn, 27.70.+q, 97.10.Cv

I. INTRODUCTION

The interpretation of the ^{187}Re decay ($t_{1/2} = 41.2$ Gyr) [1] as a potential cosmochronometer [2] relies on the fact that ^{187}Re is essentially produced by the rapid neutron capture process (r process), which occurs during supernova explosions of massive stars. The amount of ^{187}Os that was produced by the decay of ^{187}Re can be determined via the well-defined abundance patterns of the slow neutron capture process (s process). Since ^{186}Os and ^{187}Os are completely shielded from the r process by ^{186}W and ^{187}Re, and since the "local approximation" of the s process $(\langle\sigma\rangle \times N_s)_{(A)} = (\langle\sigma\rangle \times N_s)_{(A+1)}$ holds in this mass region, the ratio of their s abundances, N_s, can be obtained by their stellar (n,γ) cross sections.

The stellar (n,γ) cross sections, $\langle\sigma\rangle$, are essentially determined by averaging the energy-dependent (n,γ) cross sections measured in a time-of-flight experiment as described in Paper I [3] over the stellar neutron spectrum that is given by a Maxwell-Boltzmann distribution. However, these Maxwell-averaged cross sections (MACS) have to be corrected for the fact that the temperatures at the s-process site are high enough to create a significant population of excited states. Neutron captures on these excited states may have a different cross section than the ground state, but only the ground-state cross section is accessible by experiment.

The corresponding correction of the MACS values deduced from experimental (n,γ) cross sections has to be obtained by theoretical calculation of the capture cross sections for the relevant excited states and is expressed by the so-called stellar enhancement factor

$$\mathrm{SEF} = \frac{\langle\sigma^{\star}\rangle}{\langle\sigma^{\mathrm{lab}}\rangle}, \tag{1}$$

where $\sigma^{\star}$ and σ^{lab} indicate the MACS values under stellar and laboratory conditions.

The stellar MACS are determined by the sum of the capture cross sections of the ground state and of the relevant excited nuclear states E_i weighted by their population probabilities in the thermal photon bath,

$$p_i = \frac{(2I_i+1)\mathrm{e}^{-E_i/kT}}{\sum_m (2I_m+1)\mathrm{e}^{-E_m/kT}}, \tag{2}$$

where I_i denotes the total angular momentum. This correction is particularly important for ^{187}Os as illustrated in Fig. 1. Compared to the even neighbor isotopes ^{186}Os and ^{188}Os, there are several low-lying states in ^{187}Os, i.e., at 9.75, 74.4, 75.0, and 100.6 keV, which can be populated during the s process. At a thermal energy of $kT = 30$ keV, for example, the population probability of the 9.75-keV level reaches 43%, thus exceeding even that of the ground state (30%) because of its higher spin value [4].

Within the Hauser-Feshbach statistical model theory (HFSM) [5], the stellar neutron capture cross section is given by the sum over all excited states,

$$\sigma_{n,\gamma}(E_n) = \frac{\pi}{k_n^2}\sum_{J,\pi} g_J \frac{\sum_{ls} T_{n,ls}T_{\gamma,J}}{\sum_{ls} T_{n,ls} + \sum_{ls} T_{n',ls} + T_{\gamma,J}} W_{\gamma,J}, \tag{3}$$

where E_n is the incident neutron energy, k_n the wave number, l the orbital angular momentum of the neutron-nucleus relative motion, and $s = 1/2$ the intrinsic spin of the neutron. The statistical weighting factor for target nuclei in states of spin I and compound states of total angular momentum J compatible with spin and parity conservation laws is

$$g_J = \frac{(2J+1)}{(2s+1)(2I+1)}.$$

W_γ is a factor which takes the different statistical fluctuation properties of the γ, neutron elastic (n), and inelastic (n') decay channels into account. The transmission functions for

*Now at Physikalisch-Technische Bundesanstalt, D-38116 Braunschweig, Germany; Marita.Mosconi@ptb.de
†Now at Gesellschaft für Schwerionenforschung, D-64291 Darmstadt, Germany.

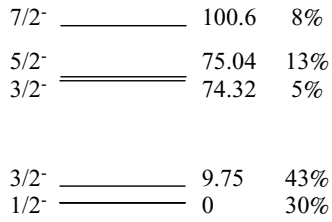

FIG. 1. Low-lying levels in ^{187}Os. Spins and excitation energies (in keV) are indicated left and right of the levels. Population probabilities (in %) are given for a thermal energy of $kT = 30$ keV, similar to the temperatures at the s-process site. Note the significance of the first excited state.

the neutron channels, T_n (elastic) and $T_{n'}$ (inelastic), can be calculated from the optical model theory of neutron-nucleus interaction. The γ-ray transmission functions, T_γ, can be derived from models of giant dipole resonance excitation combined with the Brink-Axel hypothesis and the principle of time-reversal invariance of nuclear reactions (detailed balance). Note, that Eq. (3) represents the expression for the ground state, which is adequate for the description of the experimental data. The general form including the effect of excited states is used in the calculation of the stellar enhancement factors in Paper III [6].

The neutron transmission functions T_n are related to the compound nucleus formation and can be directly derived from the ratio of the average neutron widths to the average neutron level spacing in the resolved resonance region. Similarly, the γ-ray transmission functions can be related to the ratio of the average γ-ray widths to the average neutron level spacing. Therefore, all but the inelastic transmission functions, $T_{n'}$, entering in the HFSM description can be constrained from direct experimental information. Consequently, the improvement of the inelastic cross section for the crucial first excited level in ^{187}Os adds important information on the evaluation of the Re/Os clock, in particular because it can also be used to parametrize the so-called superelastic scattering channels, which open when the target nuclei are in excited states and the inelastically scattered neutrons gain energy by de-excitation to a lower energy state of the target.

Previous measurements of the inelastic scattering cross section to the 9.75-keV level were mostly performed via direct detection of the scattered neutrons. An interesting experiment by Macklin *et al.* [7] made use of the pulsed white neutron beam at the Oak Ridge electron linac ORELA [8] by separating the inelastically scattered neutrons from the time-of-flight (TOF) window at 34.2 keV by means of the interference minimum in the total cross section of ^{56}Fe at 24.4 keV. The ratio of the elastic and inelastic cross section was determined to be 8.3 ± 0.7, yielding an inelastic cross section of 1.5 ± 0.2 barn at 34 keV.

Monoenergetic neutron beams were applied in experiments by Hershberger *et al.* [9], who used the ^{7}Li$(p,n)^7$Be reaction to produce a pulsed neutron beam of 60.5 ± 8.5 keV at full width at half maximum (FWHM). The inelastic component sitting on the low energy tail of the elastic part was separated by fitting the TOF spectra with the shape obtained with a ^{188}Os reference sample. In this case, a cross section ratio of 9.4 ± 0.4 was obtained, resulting in an inelastic-scattering cross section of 1.13 ± 0.2 b.

In a reactor-based measurement Litvinsky *et al.* [10] used an iron filter to obtain a monoenergetic neutron beam of 24.4 ± 2.1 keV at FWHM. Because the inelastically scattered neutrons from the continuous beam could not be separated from the γ background, the inelastic component was determined by subtracting the cross sections for elastic scattering and for neutron capture from the total cross section. The inelastic cross section determined in this way was 1.04 ± 0.30 b. Similarly, Litvinsky *et al.* [11] used a ^{52}Cr filter to produce a continuous beam of 45-keV neutrons with an energy spread of $\sim$7 keV FWHM. At this higher energy, the elastic and inelastic components could be separated with a spectrometric proton-recoil detector using the elastic response obtained with a lead sample. The inelastic scattering cross section at 45 keV was found to be 1.51 ± 0.45 b.

The uncertainties reported in these measurements are ranging between 13 and 30%. Compared with a theoretical prediction with the TALYS code [12] based on standard global optical model parameters (Fig. 2 and subsection IV B), the experimental results of Refs. [7,9,11] are in fair agreement with the calculated energy dependence but significantly higher. In contrast, the result of Ref. [10] is in good agreement with the theoretical prediction but deviates from the calculated energy dependence if combined with the other data. This inconsistency has been investigated in a new independent measurement that was performed at an energy close to the relevant astrophysical range.

Measurement and data analysis are described in Secs. II and III. The result is presented and discussed in Sec. IV together with the theoretical calculation.

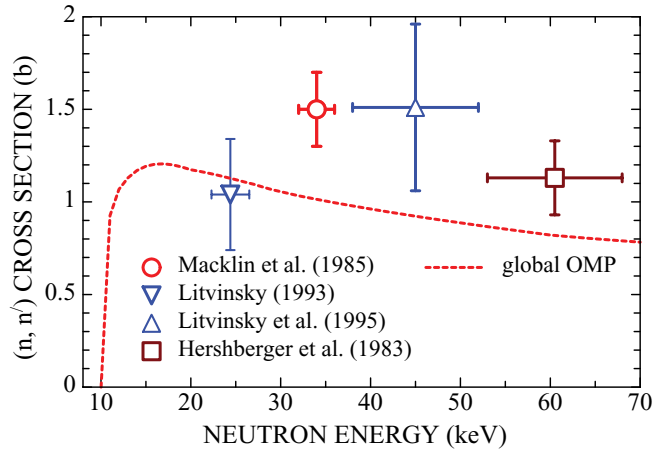

FIG. 2. (Color online) Measured inelastic-scattering cross sections for the first excited state in ^{187}Os [7,9–11] compared with a theoretical prediction performed with the TALYS code [12] and standard optical model parameters. Note that the trend with neutron energy suggested by the combined experimental data is not consistent with the calculated energy dependence.

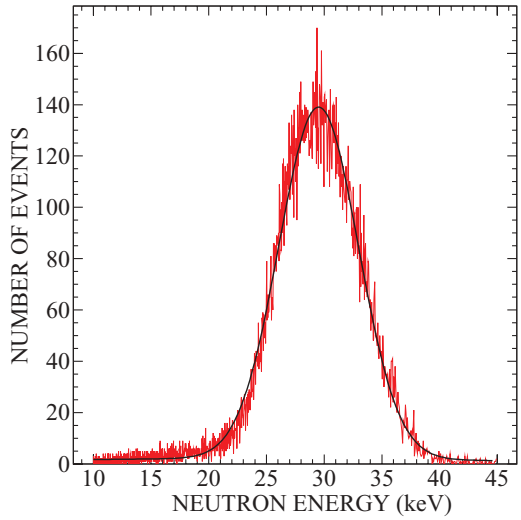

FIG. 3. (Color online) Neutron energy spectrum from the ^{7}Li$(p,n)^{7}$Be reaction at threshold. The spectrum is centered at 29.5 keV with a FWHM of 8 keV. The measurement was performed with a ^{6}Li glass detector at a flight path of 29 cm. The solid line represents a fit by the superposition of two Gaussian distributions.

II. MEASUREMENT

A. Neutron source

The present approach for the measurement of the inelastic channel was to use the ^{7}Li$(p,n)^{7}$Be reaction for producing a beam of 30 keV neutrons, close to the thermal energy of 23 keV, which is characteristic for the temperature during the He shell flashes in thermally pulsing AGB stars where the ^{186}Os/^{187}Os abundance ratio is shaped.

In a previous study it has been shown that an almost Gaussian neutron energy distribution can be obtained at the threshold of the ^{7}Li$(p,n)^{7}$Be reaction. Depending on the beam energy, spectra centered at 30 keV with a FWHM between 7 and 10 keV could be produced at the Karlsruhe 3.7-MV Van de Graaff accelerator. An example of such a spectrum is shown in Fig. 3. Narrower energy spectra could be produced as well, but at the expense of the intensity. In the present measurement, the proton energy has been restricted to a value of 0.7 keV above threshold which represents the best compromise between the width of the spectrum and the neutron yield. This limit of 0.7 keV above the threshold is already difficult to obtain and requires excellent stability of the accelerator.

At higher proton energies, a spectrum centered at 52.7 keV with a FWHM of 8.2 keV was produced as well [13], similar to the spectrum of 60.5 keV neutrons used by Hershberger *et al.* [9]. However, this distribution exhibits a pronounced tail toward lower energies, which is inherently connected with the (p,n) reaction. Because this tail interferes with the spectrum of inelastically scattered neutrons, it is more difficult to use for an accurate cross-section measurement.

The 30-keV spectrum produced at the threshold of the ^{7}Li$(p,n)^{7}$Be reaction was preferred in this work because of the good energy resolution and the smaller background at the energies of the inelastic events. A further advantage of the 30-keV spectrum is the narrow collimation provided by the reaction kinematics.

For maintaining a narrow neutron spectrum the energy stability of the accelerator is crucial. The experiment was performed at a dedicated beam line, where the object slit was located at the largest possible distance (3 m) from the analyzing magnet. In this way, the energy stability of the proton beam could be optimized without significant losses of the initial beam intensity of typically 4 to 5 μA at a 1-MHz repetition rate. However, the residual energy spread of the proton beam forced us to sacrifice about 2/3 of the beam because the maximum proton energy had to be limited to 0.7 keV above threshold.

In order to maintain stable beam conditions for several hours the neutron spectrum was monitored in intervals of 2 min and an alarm was triggered when the FWHM of the distribution exceeded the critical limit of 10 keV. In this way the width could be kept between 7.6 and 9.5 keV for runs of several hours. Furthermore, recording the data event by event allowed us to select runs of comparable FWHM during data analysis.

B. Detectors

The measurements were performed with ^{6}Li glass scintillators with an enrichment in ^{6}Li of 95% and a lithium concentration of 7.5%. This choice was made after initial tests with ZnS(Ag) scintillators, which were considered because of their appealing n/γ-discrimination capabilities. This scintillator is available in form of compressed powder. The opacity of the material is large so that the sensitive layer is limited to a fraction of a millimeter [14,15]. In commercial detectors the volume is enlarged by folding a thin sheet and mounting it on a light guide.

For the present application it turned out that the light guide was causing moderation, resulting in an additional broadening of the measured spectra by some keV compared to the spectra measured with a ^{6}Li glass scintillator [16]. If a 1-mm-thick scintillator was used instead, the efficiency was considerably smaller than that of a 1-mm-thick ^{6}Li glass scintillator. Because the detection efficiency is crucial in view of the reduced neutron yield at the threshold of the ^{7}Li$(p,n)^{7}$Be reaction, 3-mm-thick ^{6}Li glass scintillators were found to be the best choice with respect to efficiency, prompt response, and n/γ-discrimination capabilities.

C. Experimental setup

The accelerator was operated in pulsed mode with a repetition rate of 1 MHz and a pulse width of 10 ns. The target consisted of a metallic layer of natural lithium 1 μm in thickness, which was evaporated onto silver backings to reduce the background from (p,γ) reactions. Under the conditions of the present measurements, the maximum emission angle was always below 14°.

Figure 4 shows a sketch of the experimental setup. A ^{6}Li glass monitor 3 cm in diameter and 3 mm in thickness was placed at a distance of 111 cm from the lithium target. Scattered neutrons were registered by an array of three ^{6}Li-glass scintillators outside the neutron cone at a distance of 26.1 cm from the sample at angles of 90 (DET1), 120 (DET2), and

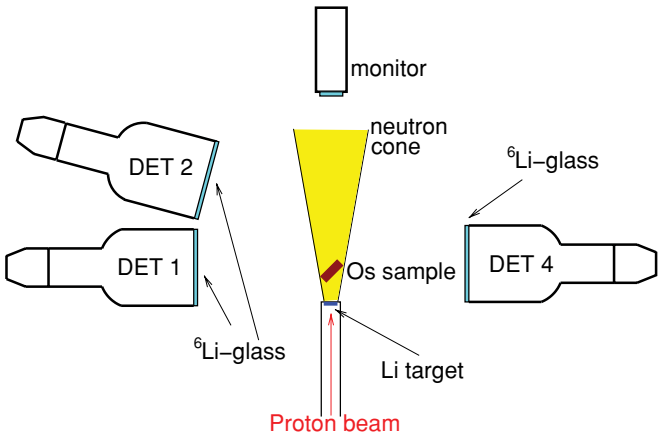

FIG. 4. (Color online) Sketch of the experimental setup (not to scale). The sample is mounted at a distance of 4 cm from the lithium target. The flight paths from the sample to the detectors are 26.1 cm and the neutron monitor is located 111 cm from the target.

270° (DET4) with respect to the beam axis. Detectors 1 and 4 were partly shielded against the γ background from the (p,γ) reactions by a shadow bar of lead (not shown in Fig. 4).

The ^{187}Os and ^{188}Os samples in this experiment are the same used in the (n,γ) measurements at CERN described in Paper I [3]. The samples were made from enriched metal powder (Table I), which was encapsulated in thin aluminum cans 15 mm in diameter and ~0.1 mm in thickness. The cans were glued to a KAPTON foil sustained by a carbon fiber frame, which was always outside the neutron cone. As indicated in Fig. 4 the samples were mounted in the center of the detector array at a distance of 4 cm from the lithium target at an angle of 45° with respect to the proton beam. The ^{188}Os sample was measured in order to obtain the spectrum of elastically scattered neutrons. In addition, an empty can was used to determine the ambient background.

The detector signals and the pick-up signal of the accelerator were recorded with fast digitizers with a sampling rate of 1 GHz. The digitized signals were subjected to an on-line software analysis described below.

The experiment was organized in 24-h runs. The three samples (^{187}Os, ^{188}Os, and the empty can) were alternatively measured to reduce systematic effects related with the accelerator conditions and the related width of the neutron spectrum. The runs were sorted according to the FWHM of the neutron distribution measured by the monitor detector. It was found that runs with a FWHM of 9.5 keV were offering the best compromise between counting statistics and background discrimination. Therefore, these runs have been used for further analysis.

In principle, it is possible to produce neutron spectra with a FWHM smaller than 8 keV, but this would require a better energy stability of the proton beam than could be achieved with our accelerator.

III. DATA ANALYSIS

The digitized detector signals were processed online to derive (i) the integral area of the signal, (ii) the ratio between the prompt and the delayed fraction of the signal for n/γ discrimination, and (iii) the time-of-flight between the pick-up signal and the detector signal of each event. First, the events were sorted by the n/γ discrimination routine based on the ratio between the prompt and the delayed signal fractions. This ratio was determined for each detector in separate calibration runs via its response to the direct neutron beam. TOF spectra were then produced from the selected events. In this step, the signal-to-background ratio was further optimized by proper choices of the discrimination thresholds. With these cuts, the γ-ray background could be reduced by a factor of 50.

As illustrated in Fig. 5 the improvement obtained by this off-line data processing was absolutely crucial for the separation between the elastic and inelastic components in the TOF spectra. Note that the TOF peak around channel 290, which corresponds to the γ flash from the impact of the proton beam on the Li target, is not much affected by the n/γ discrimination routine, whereas it works efficiently in the TOF region corresponding to neutron-induced signals beyond channel 350.

A. Processed TOF spectra

After the cuts in pulse height and the n/γ discrimination, the TOF spectra exhibit still a few background components as shown in Fig. 6. Apart from an ambient, time-independent background one finds a first peak due to (p,γ) interactions in the slits close to the lithium target followed by the dominant γ flash from the impact of the proton pulse on the target. The γ flash overlaps partly with γ rays due to neutron captures in the sample. The smaller peak at channel 370 stems from the (n,γ) resonance at 5.9 keV in the aluminum of the sample can. Then, scattered neutrons are recorded between channels 430 and 660. The weak feature at channel 800 is due to (n,γ) reactions in the monitor detector.

TABLE I. Sample characteristics.[a]

Sample	Mass (mg)	Thickness (10^{-3} atoms/b)	Isotopic composition (%)					
			186	187	188	189	190	192
^{187}Os	1921.2	3.549	1.06	70.43	12.73	5.13	5.42	5.21
^{188}Os	1996.7	3.669	0.11	0.12	94.99	2.55	1.27	0.97

[a]Os samples prepared from metal powder with a diameter of 15 mm.

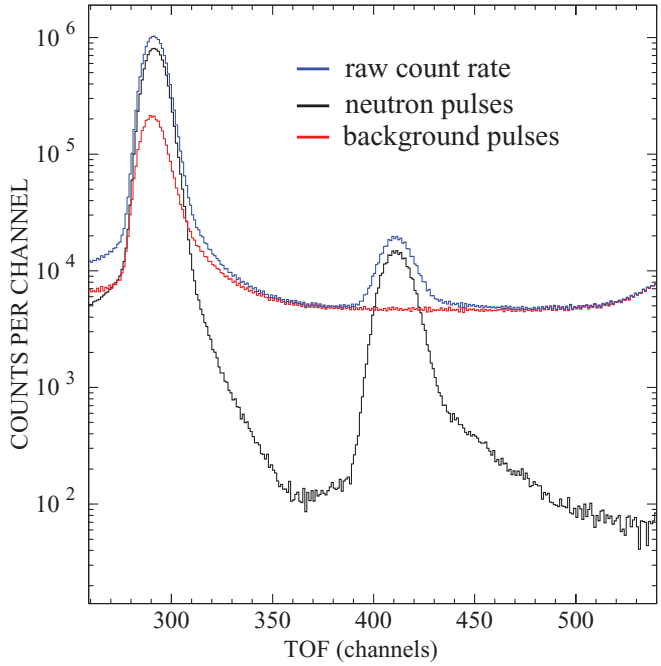

FIG. 5. (Color online) Comparison of raw and processed TOF spectra. The peak at channel 290 corresponds to the γ flash from the impact of the proton beam on the Li target and is, therefore, not much affected by the n/γ discrimination routine. In the relevant TOF region containing the events due to scattered neutrons (channels 350 to 500), however, the n/γ discrimination works efficiently.

The various background components can be discriminated by TOF or are derived from runs with the empty can. For example, the peak due to γ-rays from the 5.9 keV aluminum resonance extends slightly into the TOF region of elastically scattered neutrons. The corresponding correction has been derived from the spectrum of the empty can. The small bump due to neutron captures in the monitor detector was subtracted in the same way.

While the TOF spectra of ^{187}Os taken with DET1 and DET4 provide a clean shape for the distribution due to scattered neutrons, the spectrum measured with DET2 exhibits a large additional background superimposed with the inelastic component. The absence of this effect in the other detectors and the fact that it was much weaker for the ^{188}Os sample indicated that this background is due to a sample effect. It was eventually identified by the Monte Carlo simulations described below to result from elastic scattering on hydrogen in the glue that was used to seal the aluminum cans. According to the records from sample preparation, three times more glue was used for the ^{187}Os sample than for ^{188}Os. Because the scattering cross section of hydrogen is strongly peaked in the forward direction, this background is absent in DET1 and DET4. In view of this unexpected background, the spectra taken with DET2 were omitted from further analysis.

B. Comparative approach

The data were analyzed in two ways. In the comparative approach [7,9], the energy dependence of the elastic-scattering

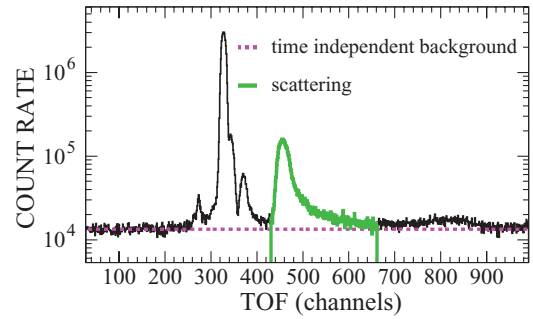

FIG. 6. (Color online) Raw TOF data of ^{187}Os taken with DET1. The time-independent background was determined left of the first peak due to (p,γ) interactions in the slits close to the lithium target. The second, prominent peak corresponds to the γ flash from the impact of the proton pulse on the target. This peak overlaps with γ rays from neutron captures in the sample. The smaller peak before the distribution produced by scattered neutrons (between channels 430 and 660) stems from the (n,γ) resonance at 5.9 keV in the aluminum of the sample can. The last feature at channel 800 is due to (n,γ) reactions in the monitor detector.

distribution has been considered to be identical for ^{187}Os and ^{188}Os. The inelastic component in ^{187}Os was determined by the difference between the measured spectrum and a fit of the elastic component using the shape of the scattering yield from the ^{188}Os sample. This method has been used in all previous measurements (sometimes even without fitting).

In this analysis the background from the aluminum can was subtracted by normalization of the spectrum taken with the empty can to match the TOF feature of the 5.9-keV aluminum resonance. The energy dependence of the detector efficiency was assumed to follow the shape of the ^{6}Li$(n,\alpha)^3$H cross section. To facilitate the fit, the TOF spectra were converted into energy spectra and the elastic component was fitted with a superposition of three Gaussian functions. The quality of the fit and the separation between elastic- and inelastic-scattering contributions are illustrated in Fig. 7 by the data taken with DET4.

The error bars in Fig. 7 are dominated by the width of the γ flash and the flight path uncertainties in the time-to-energy conversion. The energy distribution of the inelastic part has the shape of the elastic component but shifted by the 9.75 keV of the scattering state and corrected for the energy dependence of the inelastic-scattering cross section (taken from the theoretical prediction in Fig. 2). The energy shift considered also a small correction for the neutron TOF between the lithium target and the sample. The only free parameters in the fit were the relative amplitudes of the elastic and inelastic components.

The comparative analysis provided a ratio of 12.0 for the elastic and inelastic components in the spectrum of ^{187}Os. After correction for isotopic impurities, this translates into a cross-section ratio for elastic and inelastic scattering of 8.4 ± 1.2. It has to be pointed out, however, that sample related effects are neglected in the comparative analysis.

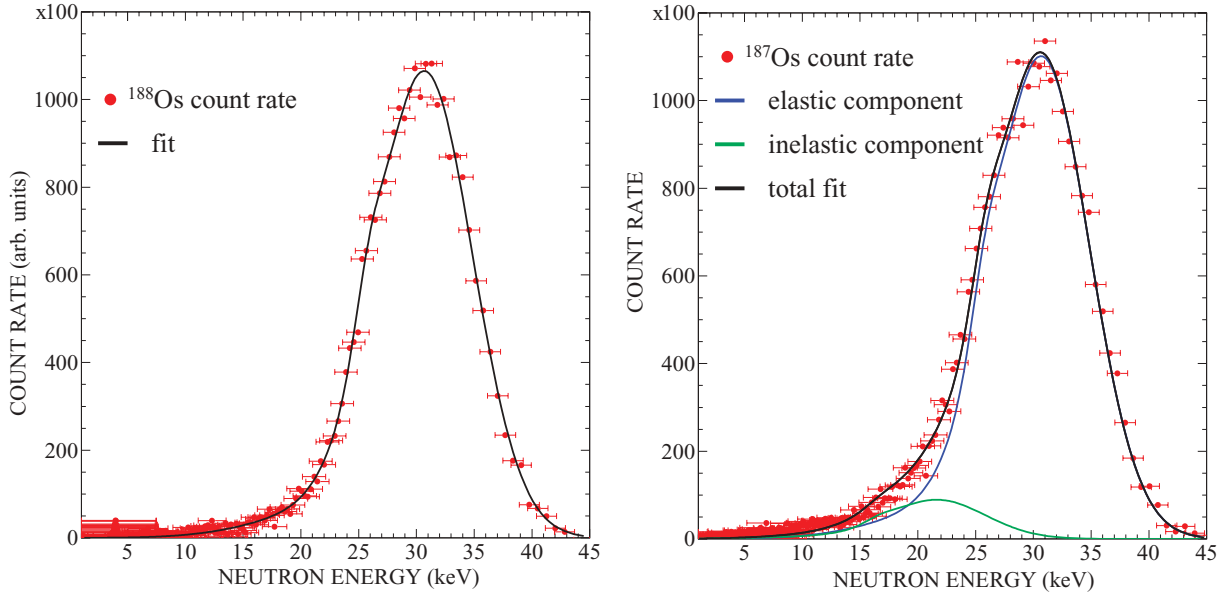

FIG. 7. (Color online) Energy spectra from DET4 for ^{188}Os and ^{187}Os. The ^{188}Os spectrum has been fitted by superposition of three Gaussian functions to reproduce the shape of the elastic-scattering yield. The shape of the inelastic part was obtained by shifting the elastic component by the 9.75-keV energy of the excited state. The fit of the ^{187}Os spectrum was performed by superposition of the two distributions and assuming the respective normalization constants as the only free parameters in the fit. The shoulder around 25 keV is due to the kinematics of the ^{7}Li$(p,n)^{7}$Be reaction.

C. Monte Carlo simulation

In a more realistic approach the scattering components in the TOF spectra of ^{187}Os and ^{188}Os were described by detailed Monte Carlo simulations for the complete geometry of the setup using the GEANT-MICAP simulation tool kit [17–19]. In this way, several experimental effects, and in particular the sample-related effects, could be considered quantitatively. Once the simulations had been verified to describe the elastic scattering of ^{188}Os properly, the elastic and inelastic components in the ^{187}Os spectrum could be determined using the same parametrization for the elastic part, whereas the inelastic component was obtained by shifting the elastic part by the 9.75 keV excitation energy of the scattering state. The cross-section ratio of elastic to inelastic scattering, which was considered as a free fit parameter, was thus defined by the relative intensities of the two components. Detailed Monte Carlo simulations to improve the uncertainties in the analysis of the ^{187}Os(n,n') cross section have been employed for the first time.

Neutrons were generated in the Li target with an energy spectrum according to the kinematics of the ^{7}Li$(p,n)^{7}$Be reaction and with the assumption of a realistic proton energy distribution. The TOF resolution was described in the simulation by the pulse width and the time response of the ^{6}Li glass detectors. The detectors, samples, and sample holder were simulated in full detail, including the amount of glue used to seal the aluminum cans. The isotopic composition of the samples and the respective total and elastic cross sections were properly considered. The detector efficiency was described via the energy dependence of the ^{6}Li$(n,\alpha)^{3}$H cross section and by modeling the mechanical parts, i.e., the photomultiplier tube, silicon oil for optical coupling, aluminum housing, and insulating tape, in detail.

The simulations allowed us to separate scattering by the osmium sample from that on any other material around the sample. In this way it could be confirmed that neutrons recorded in the detectors at 90° are almost completely due to scattering on osmium and that the broad feature in the spectra measured with DET2 was indeed caused by scattering on the hydrogen in the glue for sealing the ^{187}Os sample (Fig. 8).

The simulated spectra for elastic scattering were matching the measured ^{188}Os spectrum with a reduced χ^2 of 1.1 to 1.5. The normalization to the number of events in the TOF distribution was the only free parameter used in this fit.

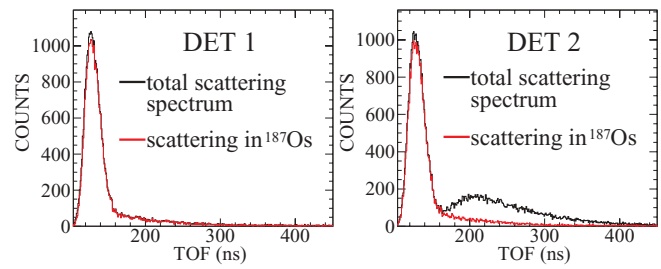

FIG. 8. (Color online) Simulated response of DET1 and DET2 to neutrons scattered by the entire ^{187}Os sample and by the ^{187}Os alone. The background due to scattering by material around the sample is very small for the detectors at 90° but rather large at lower angles (see text).

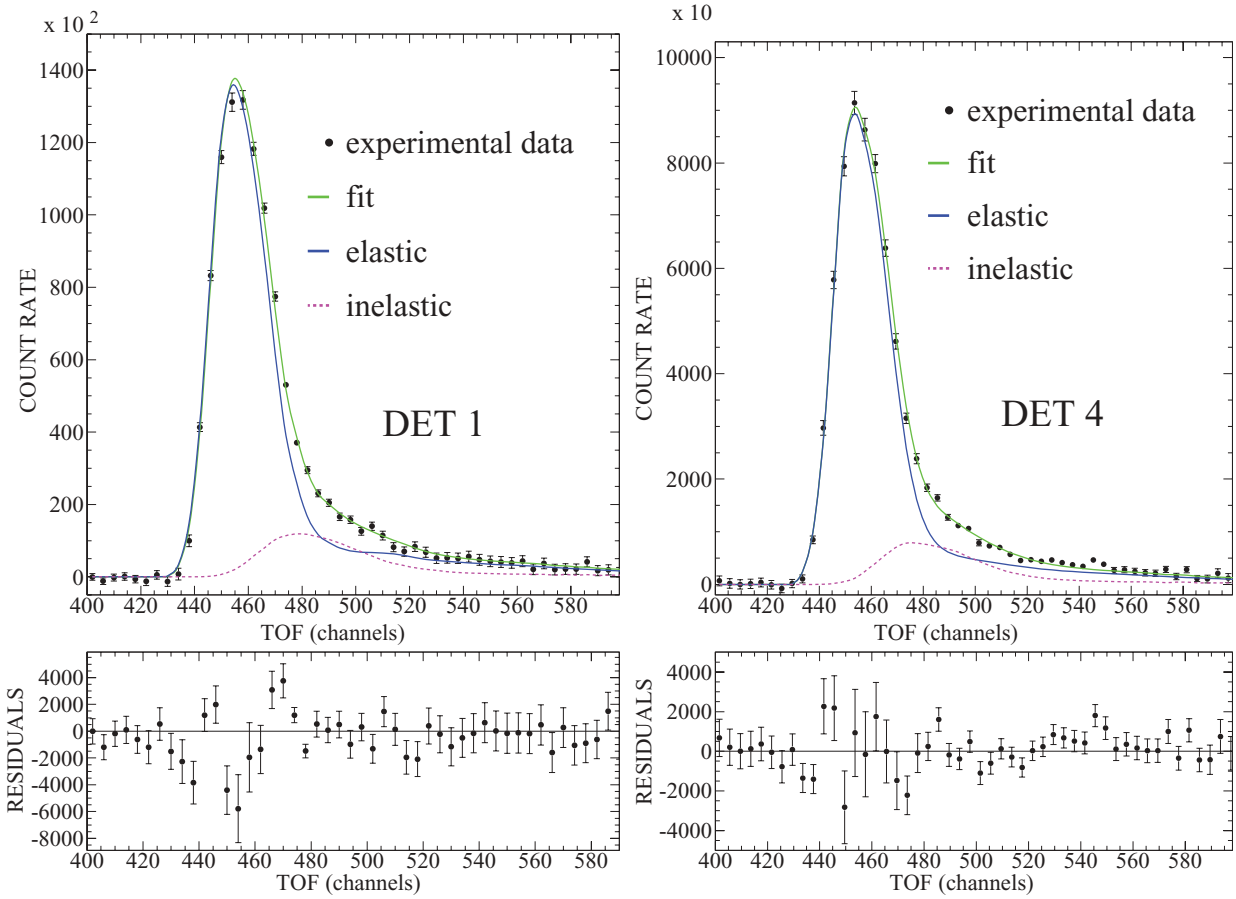

FIG. 9. (Color online) (Top) The background subtracted TOF spectrum of ^{187}Os and a Monte Carlo fit of the data with a reduced χ^2 of 1.4. (Bottom) The uncertainties of the remaining residuals are dominated by systematic uncertainties resulting from background subtraction.

The elastic and inelastic components in the ^{187}Os spectra were fixed in shape and position and only their relative normalization was treated as as a free parameter in the fits. The quality of the fits and of the separation between the elastic and inelastic component are shown in Fig. 9. Although the inelastic contribution is considerably smaller than the elastic response, it can be identified by its clear signature.

The cross-section ratio for elastic and inelastic scattering of ^{187}Os that has been determined by the Monte Carlo simulations of the spectra taken with DET1 and DET4 is 8.0 ± 0.1 and 8.1 ± 0.1, respectively, in perfect agreement with the ratio 8.4 ± 1.2 obtained in the comparative analysis. This agreement confirms the validity of the simulations and the negligible effect of the sample can in extracting the cross-section ratios.

D. Uncertainties

The uncertainties shown in Fig. 9 are clearly dominated by systematic effects. The systematic uncertainty has been obtained by comparing the cross-section ratios obtained by variation of the background contributions from the sample can and from the KAPTON foil of the sample holder within plausible ranges. While most background components identified in Fig. 6 are small and well determined, the contributions from the sample can and the KAPTON foil cannot be identified experimentally but must be evaluated by comparison of the simulated and measured spectra taken with the empty can. The corresponding uncertainty was estimated by assuming two extreme cases: (i) neglecting the background from sample can and KAPTON foil completely and (ii) increasing the adopted effect by 50%. The resulting differences in the cross-section ratio were between 5 and 6%. With an additional uncertainty of 1% for the fit procedure, which was estimated from the results obtained with DET1 and DET4, the final ratio of the elastic and inelastic component is 8.1 ± 0.5.

IV. THE (n,n') CROSS SECTION

A. Experimental values at 30 keV

The ratio of the elastic- and inelastic-scattering cross sections of ^{187}Os has been determined with a neutron energy resolution of 9.5-keV FWHM and an uncertainty of 6%. Combining the ratio of 8.1 ± 0.5 from this work with the elastic-scattering cross section of $\sigma(n,n) = 13.27 \pm 0.30$ b obtained by interpolation of data from Refs. [10,11], the

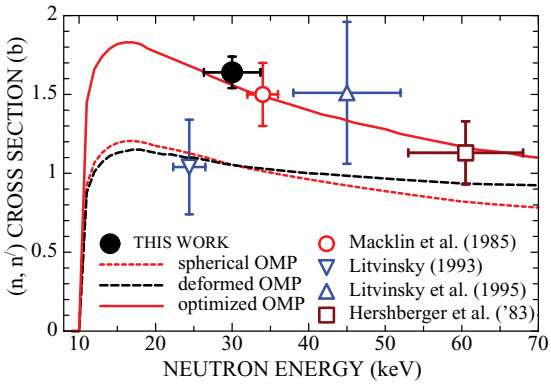

FIG. 10. (Color online) Inelastic-scattering cross sections from Refs. [7,9–11] compared to the present result. The lines refer to TALYS calculations with standard spherical OMP, coupled-channels calculations with the same OMP, and the OMP set constrained by the experimental (n,n') cross-section data.

inelastic cross section at 30 keV is

$$\sigma(n,n') = 1.64 \pm 0.10 \text{ b}.$$

With this value an ambiguity between the theoretically expected energy dependence and previous experimental data could be resolved as illustrated in Fig. 10. The present result appears to be in good agreement with the measurements reported in Refs. [7,9,11], thus confirming the calculated shape of the inelastic-scattering cross section to the 9.75-keV state. Shape and magnitude of the inelastic cross section represent valuable information for describing the competition between the (n,γ) and (n,n') channels in the statistical model calculation of the stellar capture cross section of ^{187}Os.

B. Theoretical calculations

The cross-section calculations have been performed with the Hauser-Feshbach statistical model using the TALYS code version 1.0 of Koning *et al.* [12]. First, calculations were performed with the spherical optical model of Moldauer [20], adopting the standard set of global optical model parameters (OMP) shown in Table II.

Because the Os isotopes are situated in a region of deformed nuclei, coupled-channels calculations have been performed as well to study the consequences for the cross-section shape.

TABLE II. Optical model parameters used in the Hauser-Feshbach calculations with the TALYS code [12].

Potential	Well depth (MeV)	Radius r_0 (fm)	Diffuseness[a] (fm)
V_0	46.0	1.265	0.62
W	14.0	1.352	0.25
V_{so}	7.0	1.265	0.62

[a]The diffuseness parameter of the surface absorption term was reduced by a factor of 2 to take the Gaussian shape of the Moldauer potential into account.

TABLE III. Deformation parameters used in the coupled-channels calculations.

Target	β_2	β_4
^{186}Os	0.220	−0.082
^{187}Os	0.212	−0.092
^{188}Os	0.192	−0.086

These calculations were carried out with the same OMP set used before and included the first four states of the ground-state rotational bands, i.e., the 0^+, 2^+, 4^+, and 6^+ states in the even isotopes ^{186}Os and ^{188}Os and the $1/2^-$, $3/2^-$, $5/2^-$, and $9/2^-$ states in ^{187}Os. The coupling parameters were deduced from the quadrupole and octupole deformations given in Table III.

Both calculations, which are shown in Fig. 10 by dotted and dashed lines, clearly underestimate the experimental results. Compared to the uncertainties in the experimental data, the difference between the two calculations is not significant, however. Therefore, the spherical optical model was used in search of an improved OMP set. Variation of the parameters in Table II showed that it was sufficient to change the well depth of the real part of the potential from 46 to 42 MeV for describing the measured data points without any further adjustment. The only data point that could not be reproduced refers to a very indirect measurement of the inelastic cross section [10], where the quoted uncertainties are most likely too optimistic.

The improved OMP set obtained by means of the (n,n') cross section will be complemented by the GDR and level-density parametrizations described in Paper III [6].

V. SUMMARY

The inelastic scattering cross section of ^{187}Os has been measured at a neutron energy of 30 ± 5 keV using the kinematically collimated neutron beam obtained close to the threshold of the ^{7}Li$(p,n)^7$Be reaction. The signals from a set of ^{6}Li glass detectors were recorded by fast digitizers for a detailed off-line analysis of the data.

The elastic and inelastic components in the measured time-of-flight spectra were separated by means of a careful Monte Carlo simulation with the GEANT-MICAP tool kit [17–19]. By combination of the resulting elastic/inelastic ratio of 8.1 ± 0.5 with the elastic-scattering cross section of $\sigma(n,n) = 13.27 \pm 0.30$ b obtained by interpolation of data from Refs. [10,11], the inelastic cross section at 30 keV was determined to be

$$\sigma(n,n') = 1.64 \pm 0.10 \text{ b}.$$

With this result an ambiguity in previous data could be resolved. Moreover, it could be used to adjust the OMP set for ^{187}Os that is required for calculating the cross sections from excited states, including the competition by superelastic scattering. In this way the (n,n') cross section provides valuable information for a fully consistent calculation of the stellar enhancement factor of ^{187}Os, a crucial step in the analysis of the Re/Os cosmochronometer.

[1] M. Galeazzi, F. Fontanelli, F. Gatti, and S. Vitale, Phys. Rev. C **63**, 014302 (2000).
[2] D. D. Clayton, Astrophys. J. **139**, 637 (1964).
[3] M. Mosconi, K. Fujii, A. Mengoni *et al.*, Phys. Rev. C **82**, 015802 (2010).
[4] S. E. Woosley and W. A. Fowler, Astrophys. J. **233**, 411 (1979).
[5] W. Hauser and H. Feshbach, Phys. Rev. **87**, 366 (1952).
[6] K. Fujii, M. Mosconi, A. Mengoni *et al.*, Phys. Rev. C **82**, 015804 (2010).
[7] R. L. Macklin, R. R. Winters, N. W. Hill, and J. A. Harvey, Astrophys. J. **274**, 408 (1983).
[8] P. E. Koehler (private communication).
[9] R. L. Hershberger, R. L. Macklin, M. Balakrishnan, N. W. Hill, and M. T. McEllistrem, Phys. Rev. C **28**, 2249 (1983).
[10] L. Litvinsky, A. V. Murzin, and A. M. Shkarupa, Phys. At. Nucl. **56**, 17 (1993).
[11] L. Litvinsky, Y. A. Zhigalov, V. A. Libman, A. V. Murzin, and A. M. Shkarupa, Phys. At. Nucl. **58**, 164 (1995).
[12] A. Koning, S. Hilaire, and M. C. Duijvestijn, in *International Conference on Nuclear Data for Science and Technology*, AIP Conference Series 769, edited by R. C Haight *et al.* (American Institute of Physics, New York, 2005), p. 1154.
[13] M. Mosconi *et al.*, in *Eighth International Topical Meeting on Nuclear Applications and Utilization of Accelerators* (American Nuclear Society, La Grange Park, IL, 2007), p. 807.
[14] A. R. Spowart, Brit. J. Nondestr. Test. **11**, 2 (1969).
[15] A. R. Spowart, Nucl. Instrum. Methods **75**, 35 (1969).
[16] M. Mosconi, master's thesis, University of Torino, 2002.
[17] S. Agostinelli *et al.*, Nucl. Instrum. Methods A **506**, 250 (2003).
[18] J. Johnson and T. Gabriel, Technical Report No. ORNL/TM-10340, Oak Ridge National Laboratory (unpublished).
[19] C. Zeitnitz and T. Gabriel, Nucl. Instrum. Methods A **349**, 106 (1994).
[20] P. Moldauer, Phys. Rev. C **11**, 426 (1975).